

# Retrieval of material properties of monolayer transition-metal dichalcogenides from magnetoexciton energy spectra

Duy-Nhat Ly,<sup>1,\*</sup> Dai-Nam Le,<sup>2,†</sup> Duy-Anh P. Nguyen,<sup>3</sup> Ngoc-Tram D. Hoang,<sup>1</sup> Ngoc-Hung Phan,<sup>1</sup> Hoang-Minh L. Nguyen,<sup>1</sup> and Van-Hoang Le<sup>1,‡</sup>

<sup>1</sup>*Computational Physics Key Laboratory K002, Department of Physics,*

*Ho Chi Minh City University of Education, Ho Chi Minh City 72759, Vietnam* <sup>§</sup>

<sup>2</sup>*Department of Physics, University of South Florida, Tampa, FL 33620, United States of America* <sup>§</sup>

<sup>3</sup>*The Institute of Applied Technology, Thu Dau Mot University,  
Thu Dau Mot City, Binh Duong Province, Vietnam*

(Dated: March 15, 2023)

Reduced exciton mass, polarizability, and dielectric constant of the surrounding medium are essential properties for semiconductor materials, and they can be extracted recently from the magnetoexciton energies. However, the acceptable accuracy of the previously suggested method requires very high magnetic intensity. Therefore, in the present paper, we propose an alternative method of extracting these material properties from recently available experimental magnetoexciton s-state energies in monolayer transition-metal dichalcogenides (TMDCs). The method is based on the high sensitivity of exciton energies to the material parameters in the Rytova-Keldysh model. It allows us to vary the considered material parameters to get the best fit of the theoretical calculation to the experimental exciton energies for the 1s, 2s, and 3s states. This procedure gives values of the exciton reduced mass and 2D polarizability. Then, the experimental magnetoexciton spectra compared to the theoretical calculation gives also the average dielectric constant. Concrete applications are presented only for monolayers WSe<sub>2</sub> and WS<sub>2</sub> from the recently available experimental data. However, the presented approach is universal and can be applied to other monolayer TMDCs. The mentioned fitting procedure requires a fast and effective method of solving the Schrödinger of an exciton in monolayer TMDCs with a magnetic field. Therefore, we also develop such a method in this study for highly accurate magnetoexciton energies.

## I. INTRODUCTION

Two-dimensional van der Waals semiconductors such as transition-metal dichalcogenides (TMDCs) unlock a big door to technological applications such as making ultra-thin computing devices based on their reduced dimensionality, magnetism, (opto-)spintronics, valleytronics or magneto-optics properties [1–4]. Especially magnetoexcitons in these materials provide a great potential to make light-control magnetic devices because of their thermal stability as well as their high binding energies. Hence, accurate determination of intrinsic optoelectronic quantities of these monolayer TMDCs, such as their exciton reduced mass, 2D static polarizability, or the dielectric constant of the surrounding medium, is obvious and crucial for future development of designing van-der-Waals-heterostructure-based devices.

The exciton reduced mass of monolayer TMDCs can be determined in various ways. For example, angle-resolved photoemission spectroscopy (ARPES) can experimentally detect energy vs. momentum maps and, consequently, extract the effective electron and hole masses [5–8]. However, it is an expensive and not easy-to-do method. Theoretical studies suggest more effective and

accurate ways to determine exciton reduced mass. One of the first methods is estimation from the band structure of *ab initio* calculations, such as density functional theory (DFT) [9–11]. In recent studies [12, 13], optical spectroscopy of magnetoexcitons in monolayer TMDCs has revealed exciton reduced mass. However, this method uses the diamagnetic shift to extract exciton reduced mass; thus, it requires a high magnetic intensity to reach an acceptable accuracy.

In work [13], besides the exciton reduced mass obtained from the experimental diamagnetic shift, other parameters such as the screening length (related to the 2D polarizability) and the dielectric constant of the surrounding medium are determined by comparing the experimental data for magnetoexciton energies to the theoretical calculation. Actually, the idea of comparing experimental data with theoretically calculated exciton energies to get the material properties of monolayer TMDCs was suggested early in references [14, 15]. Especially the study [15] showed that the exciton reduced mass can be extracted from the exciton energies without a magnetic field by the fitting procedure. Therefore, in the present work, we will apply this fitting scheme to the experimental data in [12, 13] as an alternative method of extracting exciton reduced mass and 2D polarizability of monolayer TMDCs. The data with the magnetic field are then used for determining the dielectric constant.

The retrieval method mentioned above requires a combination of highly accurate theoretical calculations of energy spectra and precise experimental measurements of

\* [nhatld@hcmue.edu.vn](mailto:nhatld@hcmue.edu.vn)

† [dainamle@usf.edu](mailto:dainamle@usf.edu)

‡ [hoanglv@hcmue.edu.vn](mailto:hoanglv@hcmue.edu.vn)

§ D.-N.Ly and D.-N.Le contributed equally to this work.

optical spectroscopy of excitons to archive reliable results. While the experimental data provided in [12, 13] are the most accurate measurement recently, theoretical energy spectra of the magnetoexciton are nothing but solutions of the Schrödinger equation describing a two-dimensional pair of electron and hole that interacts via Rytova-Keldysh potential because of the screening effect arising from their reduced dimensionality [10, 14, 16–19]. In the case of zero-field, these solutions can be obtained by the variational calculations [12] or semiempirical formula [20] with precision enough for analyzing experimental results. However, when a magnetic field or more accurate solutions are needed, we must use a much faster and more accurate method. Fortunately, in Ref. [15], we have provided exact numerical solutions for some  $s$  states of the exciton with and without a uniform perpendicular magnetic field with a precision of up to 20 decimal places by using the so-called Feranchuk-Komarov (FK) operator method [21, 22].

In the present study, we even improve this method more advanced by calculating the matrix elements for the Rytova-Keldysh potential using its new integral form that significantly reduces the computational resources compared with the previous version. Furthermore, examining the sensitivity of magnetoexciton energy on the material parameters allows us to establish an efficient fitting scheme from which we can accurately extract exciton reduced mass, screening length related to 2D static polarizability, and dielectric constant from experimental data of optical peaks associated with exciton  $s$ -states. Hence, a tool with universal data can be developed to extract these material properties for any monolayer TMDCs with different substrates.

Our study is organized as follows. Section II introduces solving the Schrödinger equation with Rytova-Keldysh potential using the FK operator method. Section III examines the sensitivity of exciton energy when varying exciton reduced mass and screening length and then proposes the fitting method to extract these parameters from experimental data for monolayers WSe<sub>2</sub> and WS<sub>2</sub>. In this section, the magnetoexciton energies are also used for determining the dielectric constant. Finally, Section IV devotes our conclusions.

## II. EXACT NUMERICAL SOLUTIONS FOR AN MAGNETOEXCITON IN MONOLAYER TMDC

*Schrödinger equation* – For a two-dimensional system of one electron and one hole interacting by the potential  $\hat{V}_{h-e}(r)$  in the magnetic field  $B\mathbf{e}_z$  perpendicular to the monolayer plane  $(x, y)$ , the center of mass (c.m.) motion can be separated to get the Hamiltonian for the relative motion of the electron and hole as

$$\hat{H} = \frac{\hat{p}^2}{2\mu} + \frac{1-\rho}{1+\rho} \frac{eB}{2\mu} \hat{l}_z + \frac{e^2 B^2}{8\mu} r^2 + \hat{V}_{h-e}(r) - \frac{(e\mathbf{B} \times \mathbf{K}) \cdot \mathbf{r}}{M},$$

where  $\mu = m_e^* m_h^* / (m_e^* + m_h^*)$ ,  $M = m_e^* + m_h^*$ , and  $\rho = m_e^* / m_h^*$  are the exciton reduced mass, total mass, and ratio of masses, respectively;  $m_e^*$  and  $m_h^*$  are the effective masses of electron and hole. The last term in the above Hamiltonian is the motional Stark potential with the pseudomomentum  $\mathbf{K}$  of the c.m. related to the temperature of exciton gas [23, 24]. This term can be neglected for experiments in low temperature as considered in the present study. Therefore, the Schrödinger equation for the relative motion can be written in atomic units as

$$\left\{ -\frac{1}{2} \left( \frac{\partial^2}{\partial x^2} + \frac{\partial^2}{\partial y^2} \right) + \frac{1}{8} \gamma^2 (x^2 + y^2) + \hat{V}_{h-e}(r) + \frac{1-\rho}{1+\rho} \frac{m}{2} \gamma - E \right\} \psi(x, y) = 0 \quad (1)$$

where  $r = \sqrt{x^2 + y^2}$ ; energy  $E$  and coordinates  $x, y$  are given in the effective Hartree unit  $2Ry^* = \mu e^4 / 16\pi^2 \varepsilon_0^2 \hbar^2$  and effective Bohr radius  $a_0^* = 4\pi \varepsilon_0 \hbar^2 / \mu e^2$ , respectively;  $\gamma$  is dimensionless magnetic intensity related to the magnetic field by the equation  $B = \gamma \times 2\mu \hbar Ry^* / e$ . In equation (1), the operator  $\hat{l}_z$  is replaced by its eigenvalue (the magnetic quantum number  $m$ ) because of the conservation of the angular momentum on the Oz axis.

The electron and hole interaction is described by the Rytova-Keldysh potential, initially established for excitons in thin films [16, 17] but applicable recently for excitons in monolayer TMDCs such as MoS<sub>2</sub>, MoSe<sub>2</sub>, WS<sub>2</sub>, WSe<sub>2</sub> [12, 14, 15]. In most studies, this potential is expressed via the Struve and Bessel functions and is thus suitable for numerical calculations only. For analytical calculations of the matrix elements in our approach, which significantly saves computational resources, we rewrite the Rytova-Keldysh potential by the Laplace transformation as

$$\hat{V}_{h-e}(r) = -\frac{1}{\kappa} \int_0^{+\infty} \frac{dq}{\sqrt{1 + \alpha^2 q^2}} e^{-qr}, \quad (2)$$

where the dimensionless parameter  $\alpha = r_0 / \kappa a_0^*$  is used instead of the screening length  $r_0$ . Here,  $\kappa$  is the average dielectric constant of the surrounding medium;  $r_0$  is related to the 2D static polarizability for monolayer materials by the formula  $r_0 = 2\pi \chi_{2D}$ .

*Numerical method of solving the Schrödinger equation* – The Schrödinger equation (1) can be solved numerically by several methods. In the present work, we develop a numerical method based on the matrix eigenvalue equation solver of the Linear Algebra PACKAGE (LAPACK) [25] and the Feranchuk-Komarov operator method [21, 22], where all matrix elements are calculated algebraically via the formalism of annihilation and creation operators with using the Levi-Civita transformation for two-dimensional atomic systems [26].

For this purpose, we rewrite the Schrödinger equation (1) in the algebraic form as

$$\left( -\frac{1}{8} \hat{T} + \frac{1}{8} \gamma^2 \hat{R}^3 + \hat{V} - \tilde{E} \hat{R} \right) |\psi\rangle = 0, \quad (3)$$

where all operators have the form of annihilation and creation operators as presented in Appendix A, Eqs. (A2) and (A3). Here, we use the notation  $\tilde{E} = E - \frac{1-\rho}{1+\rho} \frac{m}{2} \gamma$ . We also establish a basis set of wave vectors  $|k, m\rangle$ , Eq. (A1), labeled by a free parameter  $\omega$  and calculate all matrix elements with respect to the built basis set:  $\mathcal{R}_{jk} = \omega \langle j, m | \hat{R} | k, m \rangle$ ,  $\mathcal{T}_{jk} = \frac{1}{\omega} \langle j, m | \hat{T} | k, m \rangle$ ,  $(\mathcal{R}^3)_{jk} = \omega^3 \langle j, m | \hat{R}^3 | k, m \rangle$ , and  $\mathcal{V}_{jk} = \langle j, m | \omega \hat{V} | k, m \rangle$ . Analytical expressions for these matrix elements are given in Eqs. (A4), (A5), (A6), and (A8).

We will find the wave vector of equation (3) in the expansion via the basis set as

$$|\psi^{(s)}\rangle = \sum_{k=0}^s C_k^{(s)} |k + |m|, m\rangle, \quad (4)$$

with  $s+1$  unknown coefficients  $C_k^{(s)}$  ( $k = 0, \dots, s$ ) needed to define. For the considered system, the angular momentum  $l_z$  is conserved, so  $m$  is the magnetic quantum number and fixed; only one running index  $k$  remains. In the wave vector (4), we use only  $s+1$  basis set vectors, so that the number  $s$  can be considered an approximation order of the solutions. In practice, we will increment the  $s$ -order until getting the needed precision.

Plugging the wave vector (4) into equation (3) and acting to the left with  $\langle j, m |$  ( $j = 0, 1, 2, \dots, s$ ), we lead this equation to  $s+1$  linear equations for the coefficients  $C_k^{(s)}$  and corresponding energy  $E^{(s)}$  as

$$\sum_{k=0}^s \left( \frac{\omega^2}{8} \mathcal{T}_{jk} + \frac{\gamma^2}{8\omega^2} (\mathcal{R}^3)_{jk} + \mathcal{V}_{jk} - \tilde{E}^{(s)} \mathcal{R}_{jk} \right) C_k^{(s)} = 0, \quad (5)$$

where all matrix elements have explicit analytical expressions provided in Appendix A.

The linear equations (5) can be rewritten in the  $(s+1) \times (s+1)$  matrix eigenvalue equation, where the eigenvalue is  $\tilde{E}^{(s)}$ , while the eigenvector contains  $s+1$  elements  $C_k^{(s)}$ . This matrix eigenvalue equation can be solved using the subroutine dsygvx.f of the LAPACK.

*Exact numerical solutions* – We note that equations (5) are not solved for a sole quantum state but for a broad range of  $s+1$  quantum states with the principle quantum number  $n$  from  $|m|$  to  $|m|+s+1$ , where the magnetic quantum number  $m$  is fixed. Besides energies  $E_{nm}^{(s)}$ , our Fortran codes also give wave functions  $|\psi_{nm}\rangle$  calculated by the formula (4) with the coefficients  $C_k^{(s)}$ . The wave functions are normalized by the condition  $\sum_{j=0}^s C_j^{(s)} C_j^{(s)} = 1$ .

Generally, if  $\lim_{s \rightarrow +\infty} E^{(s)} \rightarrow E$ , the solving process converges and gives exact numerical solutions. However, in practice, we use a limited number of basis set functions to get the required precision. The more basis set functions are included in the expansion (4), the better accuracy of the solution is obtained. However, another way to increase accuracy is by choosing the appropriate value of the free parameter  $\omega$ . Work [15] shows that

convergence strongly depends on the free parameter, and there is an optimum region of the parameter where the convergence rate is highest. We confirm the same results even for the case  $m \neq 0$ , and the optimum values of  $\omega$  are implemented in the Fortran codes. Also, we consider the numerical solution exact, meaning that all the obtained digits in the solution are the right numbers; however, the obtained energies are approximate because of the approximation of the material parameters, such as the exciton reduced mass  $\mu$ , the screening length  $r_0$ , and the dielectric constant  $\kappa$ .

Tables I and II present exciton energies in monolayers WSe<sub>2</sub> and WS<sub>2</sub> encapsulated by hBN slabs for the ground and excited states with the principal quantum number  $n \leq 5$ . We provide only the  $s$ -state energies because recent experiments detect only  $s$ -state peaks in the absorption spectra. Energies for other states with  $m \neq 0$  can be calculated and are available upon request. For the calculation, the exciton reduced mass  $\mu$ , screening length  $r_0$ , and dielectric constant  $\kappa$  are taken from Table IV retrieved by our method in the next Section III.

TABLE I. Magnetoexciton energies (meV) in monolayer WSe<sub>2</sub> encapsulated by hBN slabs with  $r_0 = 4.21$  nm,  $\mu = 0.190$  m<sub>e</sub>,  $\kappa = 4.34$ . For bound energies, add the bandgap  $E_g = 1892$  meV.

Magnetic field (Tesla)	Energy (meV)				
	1s	2s	3s	4s	5s
0	-168.603	-38.568	-16.558	-9.133	-5.774
10	-168.571	-38.008	-13.887	-2.332	6.432
20	-168.473	-36.412	-7.641	10.298	25.691
30	-168.311	-33.959	0.476	25.007	46.979
40	-168.085	-30.818	9.724	40.854	69.350
50	-167.795	-27.122	19.741	57.445	92.420
60	-167.445	-22.970	30.321	74.570	115.987
70	-167.034	-18.438	41.336	92.101	139.931
80	-166.565	-13.584	52.700	109.954	164.172
90	-166.039	-8.454	64.349	128.069	188.654

TABLE II. Magnetoexciton energies (meV) in monolayer WS<sub>2</sub> encapsulated by hBN slabs with  $r_0 = 3.76$  nm,  $\mu = 0.175$  m<sub>e</sub>,  $\kappa = 4.16$ . For bound energies, add the bandgap  $E_g = 2238$  meV.

Magnetic field (Tesla)	Energy (meV)				
	1s	2s	3s	4s	5s
0	-178.617	-39.725	-16.899	-9.282	-5.853
10	-178.581	-39.096	-13.887	-1.665	7.714
20	-178.475	-37.313	-6.935	12.264	28.842
30	-178.297	-34.584	2.028	28.396	52.113
40	-178.050	-31.104	12.198	45.735	76.529
50	-177.735	-27.020	23.185	63.860	101.683
60	-177.352	-22.445	34.770	82.551	127.364
70	-176.904	-17.460	46.818	101.671	153.442
80	-176.392	-12.128	59.234	121.131	179.834
90	-175.817	-6.500	71.955	140.869	206.482

### III. RETRIEVAL OF MATERIAL PROPERTIES FROM ENERGY SPECTRA

*Sensitivity of exciton energies on material parameters* – Three parameters vary for different materials in

the Schrödinger equation (1) describing an exciton in a monolayer TMDC. They are the exciton reduced mass  $\mu$ , the screening length  $r_0$  (related to the 2D polarizability), and the average dielectric constant  $\kappa$  of the surrounding medium. Figure 1 shows the energy difference  $\Delta E_{21} = E_{2s} - E_{1s}$  dependent on  $\mu$  and  $r_0$  for monolayer TMDCs. The changes are 24 meV (18%) and 16 meV (12%), respectively, when varying exciton reduced mass in the range of  $0.16 m_e \rightarrow 0.25 m_e$  and changing screening length from 4.0 to 5.0 nm. Analogically for the energy difference  $\Delta E_{32} = E_{3s} - E_{2s}$  (not shown in the figure), the changes are 6.5 meV (30%) and 1.4 meV (6%), respectively. On another side, the measurement accuracy for exciton energies in the hBN environment is less than 1.0 meV, so the energy changes are significant enough for the experimental detection. Therefore, we conclude that exciton energies are sensitive to the change of reduced mass, screening length, and dielectric constant.

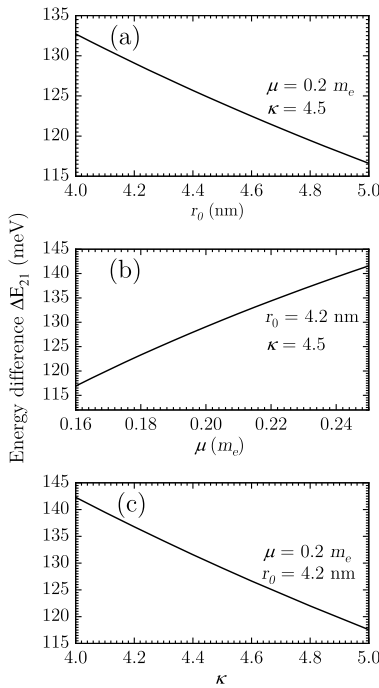


FIG. 1. Sensitivity of the exciton energy difference  $\Delta E_{21} = E_{2s} - E_{1s}$  on the exciton reduced mass (a), screening length (b), and average dielectric constant of the surrounding medium (c).

*Fitting method for exciton reduced mass, screening length, and dielectric constant* – The work of Stier *et al.* (2018) [12] for exciton energies in monolayer WSe<sub>2</sub> encapsulated by hBN slabs with  $\kappa = 4.5$  provides experimental data of 130.0 meV for energy difference  $\Delta E_{21}$  and 22.0 meV for  $\Delta E_{32}$ . This work also performs the theoretical calculation with 124.0 meV and 21.3 meV respectively for the mentioned energy differences. The discrepancies between experimental data and theoretical calculation are 4.0 % and 3.2 %, which we attribute to the inaccuracy of

the material parameters  $\mu$ ,  $r_0$ , and  $\kappa$  used in the calculation. The sensitivity of exciton energies on the material parameters inspires us to find the values of the reduced mass  $\mu$ , screening length  $r_0$ , and dielectric constant  $\kappa$  so that the theoretical results best fit the experimental data.

Figure 2 shows the relative discrepancy between the experimental data from Ref. [12] and the theoretical energy differences. We calculate it by the formula

$$\delta = \frac{1}{2} \left( \frac{|\Delta E_{21}^{\text{theo}} - \Delta E_{21}^{\text{exp}}|}{\Delta E_{21}^{\text{exp}}} + \frac{|\Delta E_{32}^{\text{theo}} - \Delta E_{32}^{\text{exp}}|}{\Delta E_{32}^{\text{exp}}} \right) \quad (6)$$

varying the exciton reduced mass  $\mu$  and screening length  $r_0$  by the steps  $\Delta\mu = 0.0025 m_e$  and  $\Delta r_0 = 0.025$  nm while fixing the value  $\kappa = 4.5$ . There is a minimum discrepancy at  $\mu = 0.204 m_e$  and  $r_0 = 4.21$  nm, which gives true values for the exciton reduced mass and screening length (2D polarizability) of the considered monolayer WSe<sub>2</sub>.

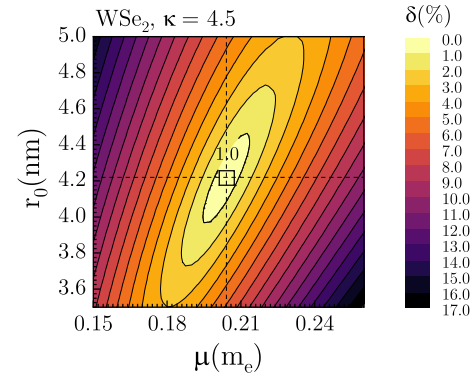


FIG. 2. Relative discrepancy between the experimental data for monolayer WSe<sub>2</sub> [12] and theoretical energy differences  $\Delta E_{21}$  and  $\Delta E_{32}$ , calculated with varied exciton reduced mass  $\mu$ , screening length  $r_0$ , and fixed  $\kappa = 4.5$ . There is a minimum at  $\mu = 0.204 m_e$  and  $r_0 = 4.21$  nm.

Mathematically, the minimum in Fig. 2 can be understood because there are two constraints ( $\Delta E_{21}$  and  $\Delta E_{32}$ ) for two parameters ( $\mu$  and  $r_0$ ) to be defined. However, we also provide a more comprehensible explanation demonstrated in Fig. 3. Panel (a) presents the energy difference  $\Delta E_{21}$  dependent on  $\mu$  and  $r_0$ , which is not monosemantic. Each energy difference value corresponds to a set of values  $\mu$  and  $r_0$ , establishing a curved line in the diagram. Analogically, Panel (b) shows a similar picture – each energy difference value  $\Delta E_{32}$  corresponds to a curved line in the plane ( $\mu$ ,  $r_0$ ). As shown in Panel (c), the two lines ( $\Delta E_{21} = 130.0$  meV and  $\Delta E_{32} = 22.0$  meV) intersect at one point, defining the material parameters for monolayer WSe<sub>2</sub>,  $\mu = 0.204 m_e$  and  $r_0 = 4.21$  nm, consistent with the results shown in Fig. 2.

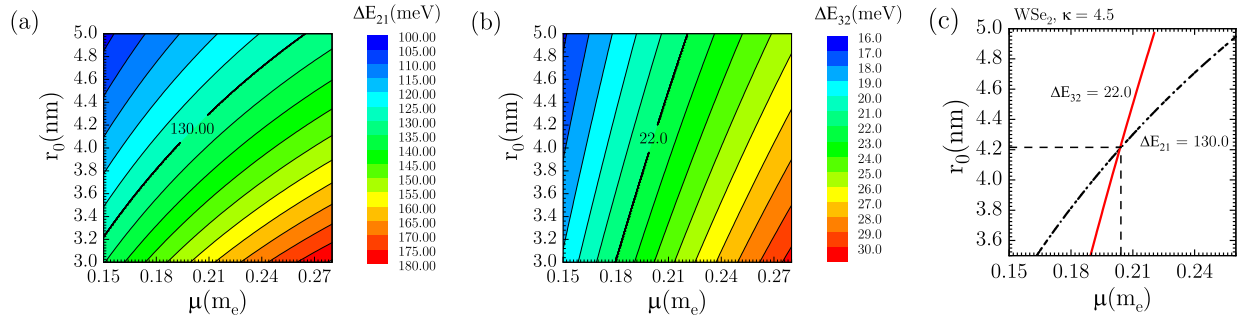


FIG. 3. Sensitiveness of the exciton energy differences (a)  $\Delta E_{21} = E_{2s} - E_{1s}$  and (b)  $\Delta E_{32} = E_{3s} - E_{2s}$  on the exciton reduced mass  $\mu$  and the screening length  $r_0$ . The energies are calculated for  $\kappa = 4.5$ . (c) The intersection of two lines ( $\Delta E_{21} = 130.0$  meV and  $\Delta E_{32} = 22.0$  meV) gives the finding values of  $\mu$  and  $r_0$ .

Work [12] also provides exciton energy spectra dependent on the magnetic intensity. We can use this information to get a more precise value of the dielectric constant  $\kappa$  of the surrounding medium (hBN in this case). First, we change  $\kappa$  around the value 4.5, from 4.0 to 5.0, and for each value  $\kappa$ , get the optimum values of  $\mu$  and  $r_0$  by the above procedure. The results presented in Table III show that the screening length does not change but is around the value of  $r_0 = 4.21$ . For each pair of optimum values of  $\mu$  and  $\kappa$ , we calculate energies for  $1s$ ,  $2s$ ,  $3s$ , and  $4s$  states of the exciton at the magnetic intensity for which the experimental energies are available in Ref. [12]. By the least square method, we get the values of  $\mu = 0.190 \text{ m}_e$  and  $\kappa = 4.34$ , where the theoretical energies best fit the experimental data. For illustration, we present in Fig. 4 exciton energy spectra calculated for two sets of  $\mu$ ,  $r_0$ , and  $\kappa$ , compared with the experimental data (color figure lines). It is clear that the theoretical spectrum best fits the experimental data at the optimum values  $\mu$ ,  $r_0$ , and  $\kappa$ .

TABLE III. Optimum values of exciton reduced mass  $\mu$  and screening length  $r_0$  extracted with different values of dielectric constant  $\kappa$ .

Dielectric constant $\kappa$	Exciton reduced mass $\mu$ ( $\text{m}_e$ )	Screening length $r_0$ (nm)
5.0	0.252	4.208
4.8	0.232	4.208
4.6	0.213	4.208
4.5	0.204	4.208
4.4	0.195	4.209
4.35	0.191	4.209
4.34	0.190	4.209
4.33	0.189	4.209
4.3	0.186	4.209
4.2	0.178	4.209
4.1	0.169	4.207
4.0	0.161	4.209

*Extracted fundamental optoelectronic material parameters for monolayer TMDCs* – The method suggested above can retrieve the reduced mass, screening length,

and dielectric constant of any monolayer TMDC from

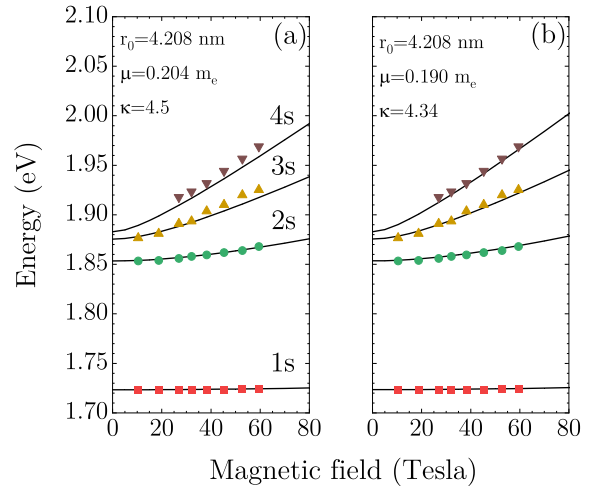


FIG. 4. Magnetoexciton energy spectra calculated with different values of material parameters: (a)  $\mu = 0.204 \text{ m}_e$ ,  $r_0 = 4.208 \text{ nm}$ , and  $\kappa = 4.5$ ; (b)  $\mu = 0.190 \text{ m}_e$ ,  $r_0 = 4.208 \text{ nm}$ , and  $\kappa = 4.34$ . The results in (b) agree better with the experimental data of Ref. [12], indicated by the color figure lines. For the bound energies in the figures, the bandgap  $E_g = 1.892 \text{ eV}$  is used.

the measured energy differences  $\Delta E_{21}$  and  $\Delta E_{32}$  combined with the magnetoexciton energy spectra. For this task, we have Fortran codes available upon request. Here, we demonstrate the method for the experimental data extracted from Ref. [12] for monolayer WSe<sub>2</sub>:  $\Delta E_{21} = 130.0$  meV,  $\Delta E_{32} = 22.0$  meV; and from Ref. [13] for monolayer WS<sub>2</sub>:  $\Delta E_{21} = 139.2$  meV,  $\Delta E_{32} = 22.1$  meV. The retrieved exciton reduced masses, screening lengths, and dielectric constants are given in Table III compared with data from other works. For reference, we also calculate the diamagnetic coefficient and exciton radius for  $1s$ ,  $2s$ , and  $3s$  states presented in the Table.

TABLE IV. Fundamental optoelectronic material parameters extracted in the present work compared with data in other references.

Material	$\kappa$	$\mu$ ( $m_e$ )	$r_0$ (nm)	$\sigma$ ( $\mu\text{eV}/\text{T}^2$ )	$r_{1s}$ (nm)	$r_{2s}$ (nm)	$r_{3s}$ (nm)	Reference
WSe <sub>2</sub>	4.34	0.190	4.21	0.28	1.68	7.01	16.09	present work
	4.5	0.20	4.5	0.32	1.7	6.6	14.3	[12]
	3.97	0.20	5.0	0.24	1.6	—	—	[27]
	2.25	0.22	4.51	0.25	1.6	—	—	[28]
	3.3	0.18	4.5	0.32	1.62	—	—	[29]
WS <sub>2</sub>	4.16	0.175	3.76	0.34	1.69	7.13	16.49	present work
	4.35	0.175	3.4	0.4	1.8	—	—	[13]
	4.5	0.15	4.0	—	2.45	—	—	[30]
	1.0	0.16	5.4	0.32	1.53	—	—	[31]
	1.55	0.15	—	0.90	2.5	—	—	[32]

#### IV. CONCLUSION

We have shown the sensitivity of the exciton energy differences among three exciton quantum states ( $1s$ ,  $2s$ , and  $3s$ ) in the monolayer TMDCs to the material properties. It inspires us to propose a method to retrieve the exciton reduced mass, screening length (related to the 2D polarizability), and dielectric constant of the surrounding medium from experimental magnetoexciton energies available recently. Applying the proposed method to monolayers WSe<sub>2</sub> and WS<sub>2</sub>, we have obtained results for the material properties that complement well the available data. The method could be extended for other monolayer TMDCs, such as MoS<sub>2</sub>, MoSe<sub>2</sub>, and MoTe<sub>2</sub>, which are the subject of recent intensive investigation.

For the mentioned-above investigation, we have developed an effective method for solving the Schrödinger equation of a magnetoexciton in a monolayer TMDC. The method gives a very fast and convergent procedure to get highly accurate magnetoexciton energies and wave functions suitable for the fitting method, which usually requires a huge data generation. Besides, all matrix elements for the Hamiltonian are obtained in analytical expressions that may be useful for further investigation of analytical magnetoexciton energies as functions of material parameters.

Fortran codes for magnetoexciton energy spectra in monolayer TMDCs are available upon request and will be published elsewhere.

#### ACKNOWLEDGMENTS

D.-N.Ly and N.-H.P. are funded by Ho Chi Minh City University of Education Foundation for Science and Technology under grant numbers CS.2019.19.43TD and CS.2019.19.44TD. This work is funded by Foundation for Science and Technology of Vietnam Ministry of Education and Training under grant number B2022-SPS-09-VL. This work was carried out by the high-performance cluster at Ho Chi Minh City University of Education, Vietnam.

#### Appendix A: Analytical matrix elements

For more effectively solving the Schrödinger equation (1), we first rewrite it in the  $(u, v)$  space by the Levi-Civita transformation  $x = u^2 - v^2$ ,  $y = 2uv$ , where the interaction potential in the  $(u, v)$  space is defined as  $\hat{V}(u, v) = (u^2 + v^2) \hat{V}_{h-e}$ . The distance and angular momentum have the compact form  $r = u^2 + v^2$  and  $\hat{l}_z = -\frac{i}{2} (v \frac{\partial}{\partial u} - u \frac{\partial}{\partial v})$ . More about the application of the Levi-Civita transformation to two-dimensional atomic systems can also be found in Ref. [26].

One advantage of using the equation in  $(u, v)$  space is to apply the algebraic formalism via annihilation and creation operators  $\hat{a}(\omega)$ ,  $\hat{a}^+(\omega)$ ,  $\hat{b}(\omega)$ , and  $\hat{b}^+(\omega)$ , where the calculation technique is based on the commutation relations  $[\hat{a}, \hat{a}^+] = 1$ ,  $[\hat{b}, \hat{b}^+] = 1$ , and the basis vectors can be presented in the form

$$|k, m\rangle = \frac{1}{\sqrt{(k+m)!(k-m)!}} (\hat{a}^+)^{k+m} (\hat{b}^+)^{k-m} |0(\omega)\rangle \quad (A1)$$

with the vacuum state  $|0(\omega)\rangle$  defined by the equations  $\hat{a}|0(\omega)\rangle = 0$ ,  $\hat{b}|0(\omega)\rangle = 0$ .

Using the annihilation and creation operators, we can rewrite all the terms in the Schrödinger equation as

$$\begin{aligned} \hat{T} &= \frac{\partial^2}{\partial u^2} + \frac{\partial^2}{\partial v^2} = \omega \left( \hat{a}\hat{b} + \hat{a}^+\hat{b}^+ - \hat{a}^+\hat{a} - \hat{b}^+\hat{b} - 1 \right), \\ \hat{R} &= u^2 + v^2 = \frac{1}{\omega} \left( \hat{a}\hat{b} + \hat{a}^+\hat{b}^+ + \hat{a}^+\hat{a} + \hat{b}^+\hat{b} + 1 \right). \end{aligned} \quad (A2)$$

Particularly, the interaction potential can be rewritten as

$$\hat{V}(u, v) = -\frac{1}{\kappa} \int_0^{+\infty} \frac{dq}{\sqrt{1 + \alpha^2 q^2}} e^{-q\hat{R}} \hat{R}. \quad (A3)$$

With the algebraic forms (A2) and (A3), we can easily calculate all matrix elements just using the commutation relations of the annihilation and creation operators. Detailed calculation method can be found in monograph [22]. Here, in this Appendix, we provide only the results

for the matrix elements. They are as follows

$$\begin{aligned} \mathcal{R}_{jk} &= \omega \langle j, m | \hat{R} | k, m \rangle = 2k \delta_{jk} + \sqrt{k^2 - m^2} \delta_{j,k-1} \\ &+ \sqrt{(k+1)^2 - m^2} \delta_{j,k+1}, \end{aligned} \quad (\text{A4})$$

$$\begin{aligned} \mathcal{T}_{jk} &= \frac{1}{\omega} \langle j, m | \hat{T} | k, m \rangle = 2k \delta_{jk} - \sqrt{k^2 - m^2} \delta_{j,k-1} \\ &- \sqrt{(k+1)^2 - m^2} \delta_{j,k+1}, \end{aligned} \quad (\text{A5})$$

$$\begin{aligned} (\mathcal{R}^3)_{jk} &= \omega^3 \langle j, m | \hat{R}^3 | k, m \rangle \\ &= 2(5k^2 + 5k + 3 - 3m^2)(2k+1) \delta_{jk} \\ &+ 6(5k^2 - 5k + 3 - 3m^2) \sqrt{k^2 - m^2} \delta_{j,k-1} \\ &+ 3(2k-1) \sqrt{k^2 - m^2} \sqrt{(k-1)^2 - m^2} \delta_{j,k-2} \\ &+ \sqrt{k^2 - m^2} \sqrt{(k-1)^2 - m^2} \sqrt{(k-2)^2 - m^2} \delta_{j,k-3} \\ &+ 6(5k^2 + 5k + 3 - 3m^2) \sqrt{(k+1)^2 - m^2} \delta_{j,k+1} \\ &+ 3(2k+3) \sqrt{(k+1)^2 - m^2} \sqrt{(k+2)^2 - m^2} \delta_{j,k+2} \\ &+ \sqrt{(k+1)^2 - m^2} \sqrt{(k+2)^2 - m^2} \\ &\times \sqrt{(k+3)^2 - m^2} \delta_{j,k+3} \end{aligned} \quad (\text{A6})$$

Here, we use the Kronecker delta  $\delta_{jk}$ .

Differently, it is not trivial to calculate matrix elements of the operator  $\hat{V}$ . However, by using the technique of constructing operators in a normal form of annihilation and creation operators, given in Ref. [22] (pages 232-233), we have formula

$$\begin{aligned} e^{-q(\hat{a}\hat{b}+\hat{a}^+\hat{b}^++\hat{a}^+\hat{a}+\hat{b}^+\hat{b}+1)} &= e^{-\frac{q}{1+q}\hat{a}^+\hat{b}^+} \\ &\times e^{-\ln(1+q)(\hat{a}^+\hat{a}+\hat{b}^+\hat{b}+1)} e^{-\frac{q}{1+q}\hat{a}\hat{b}}. \end{aligned} \quad (\text{A7})$$

With this operator in this normal form, we can apply the algebraic technique to get

$$\begin{aligned} \mathcal{V}_{jk} &= \langle j, m | \omega \hat{V} | k, m \rangle \\ &= (2k+1) U_{jk} + \sqrt{k^2 - m^2} U_{j,k-1} \\ &+ \sqrt{(k+1)^2 - m^2} U_{j,k+1} \end{aligned} \quad (\text{A8})$$

with

$$\begin{aligned} U_{jk} &= -\frac{1}{\kappa \alpha} \sum_{s=|m|}^{\min(k,j)} \sum_{t=0}^{j+k-2s} (-1)^{j+k+t} \binom{j+k-2s}{t} \\ &\times \sqrt{\binom{j+m}{s+m}} \sqrt{\binom{j-m}{s-m}} \sqrt{\binom{k+m}{s+m}} \sqrt{\binom{k-m}{s-m}} \\ &\times \int_0^{+\infty} \frac{dq}{(1+q)^{2s+t+1} \sqrt{q^2 + 1/\omega^2 \alpha^2}}, \end{aligned} \quad (\text{A9})$$

where  $\binom{n}{k} = \frac{n!}{(n-k)!k!}$  is a binomial coefficient.

In Eq. (A9), the definite integrals

$$J_p(x) = \int_0^{+\infty} \frac{dq}{(1+q)^p \sqrt{q^2 + x^2}}$$

with  $p \geq 1$  and  $x = 1/\omega\alpha > 0$  are easy to calculate numerically. Besides, for an analytical formulation, we can derive an iterative formula for these integrals as follows

$$J_p = \frac{(2p-3)J_{p-1} - (p-2)J_{p-2} + x}{(x^2 + 1)(p-1)} \quad (\text{A10})$$

for  $p \geq 2$ , where  $J_1(x)$  has the following explicit formula

$$J_1(x) = \frac{\ln(x + \sqrt{x^2 + 1}) + \ln(1 + \sqrt{x^2 + 1}) - \ln(x)}{\sqrt{x^2 + 1}}.$$

Noting that although  $J_0(x)$  is divergent, relation (A10) is still valid for  $p = 2$  by considering the limit

$$\lim_{p \rightarrow 0} p J_p(x) = 1$$

so that

$$J_2(x) = \frac{J_1(x) - 1 + x}{x^2 + 1}.$$

---

[1] A. K. Geim and I. V. Grigorieva, *Nature* **499**, 419 (2013).  
[2] A. Arora, *J. Appl. Phys.* **129**, 120902 (2021).  
[3] D. Thi-Xuan Dang, R. K. Barik, M.-H. Phan, and L. M. Woods, *J. Phys. Chem. Lett.* **13**, 8879 (2022).  
[4] M.-H. Phan, V. Kalappattil, V. O. Jimenez, Y. Thi Hai Pham, N. W. Mudiyanselage, D. Dettem, C.-M. Hung, A. Chanda, and T. Eggers, *J. Alloys Compd.* **937**, 168375 (2023).  
[5] D. N. Basov, M. M. Fogler, A. Lanzara, F. Wang, and Y. Zhang, *Rev. Mod. Phys.* **86**, 959 (2014).  
[6] F. Bussolotti, J. Yang, H. Kawai, J. Y. Chee, and K. E. J. Goh, *Phys. Rev. B* **103**, 045412 (2021).  
[7] W. Lee, Y. Lin, L.-S. Lu, W.-C. Chueh, M. Liu, X. Li, W.-H. Chang, R. A. Kaindl, and C.-K. Shih, *Nano Lett.* **21**, 7363 (2021).  
[8] Y. Lin, Y.-h. Chan, W. Lee, L.-S. Lu, Z. Li, W.-H. Chang, C.-K. Shih, R. A. Kaindl, S. G. Louie, and A. Lanzara, *Phys. Rev. B* **106**, L081117 (2022).  
[9] D. Xiao, G.-B. Liu, W. Feng, X. Xu, and W. Yao, *Phys. Rev. Lett.* **108**, 196802 (2012).  
[10] T. C. Berkelbach, M. S. Hybertsen, and D. R. Reichman, *Phys. Rev. B* **88**, 045318 (2013).  
[11] A. Kormányos, G. Burkard, M. Gmitra, J. Fabian, V. Zólyomi, N. D. Drummond, and V. Fal'ko, *2D Mater.* **2**, 022001 (2015).  
[12] A. V. Stier, N. P. Wilson, K. A. Velizhanin, J. Kono, X. Xu, and S. A. Crooker, *Phys. Rev. Lett.* **120**, 057405 (2018).  
[13] M. Goryca, J. Li, A. V. Stier, T. Taniguchi, K. Watanabe, E. Courtade, S. Shree, C. Robert, B. Urbaszek, X. Marie, and S. A. Crooker, *Nat. Commun.* **10**, 4172 (2019).  
[14] A. Chernikov, T. C. Berkelbach, H. M. Hill, A. Rigosi, Y. Li, O. B. Aslan, D. R. Reichman, M. S. Hybertsen,

and T. F. Heinz, *Phys. Rev. Lett.* **113**, 076802 (2014).

[15] D.-A. P. Nguyen, D.-N. Ly, D.-N. Le, N.-T. D. Hoang, and V.-H. Le, *Physica E* **113**, 152 (2019).

[16] N. S. Rytova, *Mosc. Univ. Phys. Bull.* **3**, 30 (1967).

[17] L. V. Keldysh, *JETP Lett.* **29**, 658 (1979).

[18] E. Hanamura, N. Nagaosa, M. Kumagai, and T. Takagahara, *Mater. Sci. Eng. B* **1**, 255 (1988).

[19] P. Cudazzo, I. V. Tokatly, and A. Rubio, *Phys. Rev. B* **84**, 085406 (2011).

[20] H. T. Nguyen-Truong, *Phys. Rev. B* **105**, L201407 (2022).

[21] I. Feranchuk and L. Komarov, *Phys. Lett. A* **88**, 211 (1982).

[22] I. Feranchuk, A. Ivanov, V.-H. Le, and A. Ulyanenkov, *Non-perturbative Description of Quantum Systems* (Springer, Switzerland, 2015).

[23] D. N.-T. Hoang, D.-N. Ly, and V.-H. Le, *Phys. Rev. B* **115**, 127401 (2020).

[24] D.-N. Ly, D.-N. Le, N.-H. Phan, and V.-H. Le, The thermo-induced effect on magneexciton energy spectra in monolayer transition-metal dichalcogenides (2022) [arxiv: 2209.13682](https://arxiv.org/abs/2209.13682).

[25] Netlib.org. LAPACK: Linear Algebra PACKage, Subroutine `dsygvx.f`.

[26] L. V. Hoang and N. T. Giang, *J. Phys. A: Math. Gen.* **26**, 1409 (1993).

[27] E. Liu, J. van Baren, T. Taniguchi, K. Watanabe, Y.-C. Chang, and C. H. Lui, *Phys. Rev. B* **99**, 205420 (2019).

[28] S.-Y. Chen, Z. Lu, T. Goldstein, J. Tong, A. Chaves, J. Kunstmann, L. S. R. Cavalcante, T. Woźniak, G. Seifert, D. R. Reichman, T. Taniguchi, K. Watanabe, D. Smirnov, and J. Yan, *Nano Lett.* **19**, 2464 (2019).

[29] A. V. Stier, N. P. Wilson, G. Clark, X. Xu, and S. A. Crooker, *Nano Lett.* **16**, 7054 (2016).

[30] J. Zipfel, J. Holler, A. A. Mitioglu, M. V. Ballottin, P. Nagler, A. V. Stier, T. Taniguchi, K. Watanabe, S. A. Crooker, P. C. M. Christianen, T. Korn, and A. Chernikov, *Phys. Rev. B* **98**, 075438 (2018).

[31] A. V. Stier, K. M. McCreary, B. T. Jonker, J. Kono, and S. A. Crooker, *Nat. Commun.* **7**, 10643 (2016).

[32] G. Plechinger, P. Nagler, A. Arora, A. Granados del Águila, M. V. Ballottin, T. Frank, P. Steinleitner, M. Gmitra, J. Fabian, P. C. M. Christianen, R. Bratschitsch, C. Schüller, and T. Korn, *Nano Lett.* **16**, 7899 (2016).